NMR Characterization of Lanthanide(3+) Complexes of Tetraazatetrakisphosphinato and Tetraazatetrakisphosphonato Ligands

by **Giovannia A. Pereira**[a]), **Laura Ball**[b]), **A. Dean Sherry**[b])[c]), **Joop A. Peters**[d]), and **Carlos F. G. C. Geraldes***[a])

[a]) Department of Biochemistry, Faculty of Science and Technology, and Center of Neurosciences and Cell Biology, University of Coimbra, PT-3001-401 Coimbra

[b]) Department of Chemistry, The University of Texas at Dallas, P. O. Box 830688, Richardson, TX 75083-0688, USA

[c]) Advanced Imaging Research Center, University of Texas Southwestern Medical Center at Dallas, 5801 Forest Park Rd., Dallas, TX 75235-9085, USA

[d]) Laboratory of Biocatalysis and Organic Chemistry, Department of Biotechnology, Delft University of Technology, Julianalaan 136, NL-2628BL Delft

Dedicated to Prof. *Jean-Claude Bünzli* on the occasion of his retirement from the EPFL, CH-Lausanne

The three-dimensional structures in aqueous solution of the entire series of the Ln^{3+} complexes $[Ln(DOTP^*\text{-}Et)]^-$ (formed from the free ligand *P*,*P*′,*P*″,*P*‴-[1,4,7,10-tetraazacyclododecane-1,4,7,10-tetrayltetrakis(methylene)]tetrakis[*P*-ethylphosphinic acid] (H_4DOTP^*-Et) were studied by NMR techniques to rationalize the parameters governing the relaxivity of the Gd^{3+} complex and evaluate its potential as MRI contrast agent. From the ^1H- and ^{31}P-NMR lanthanide-induced-shift (LIS) values, especially of the $[Yb(DOTP^*\text{-}Et)]^-$ complex, it was concluded that the $[Ln(DOTP^*\text{-}Et)]^-$ complexes adopt in solution twisted square antiprismatic coordination geometries which change gradually their coordination-cage structure along the lanthanide series. These complexes have no inner-sphere-H_2O coordination, and preferentially have the (*R*,*R*,*R*,*R*) configuration of the P-atoms in the pendant arms. Self-association was observed in aqueous solution for the tetraazatetrakisphosphonic acid ester complexes $[Ln(DOTP^*\text{-}OEt)]^-$ (= $[Ln(DOTP\text{-}Et)]^-$) and $[Ln(DOTP^*\text{-}OBu)]^-$ (= $[Ln(DOTP\text{-}Bu)]^-$) at and above 5 mM concentration, through analysis of ^{31}P-NMR, EPR, vapor-pressure-osmometry, and luminescence-spectroscopic data. The presence of the cationic detergent cetylpyridinium chloride (CPC; but not of neutral surfactants) shifts the isomer equilibrium of $[Eu(DOTP^*\text{-}OBu)]^-$ to the (*S*,*S*,*S*,*S*) form which selectively binds to the cationic micelle surface.

1. Introduction. – The use of magnetic-resonance imaging (MRI) as a clinical diagnostic tool is significantly extended by administration of contrast agents (CAs) [1]. All the clinically approved agents based on Gd^{3+} chelates have one inner-sphere H_2O molecule directly coordinated to the metal ion that exchanges rapidly with bulk H_2O. The research undertaken to achieve the important goal of optimizing the efficacy (relaxivity) of CAs has led to a much better understanding of the parameters governing it [2–6]. Careful ligand design has enabled tuning of some of these parameters to maximize the r_1 relaxivity (defined as the enhancement of the water-proton T_1 relaxation rate in 1 mM solution of CA). These parameters, namely the rotational correlation time (τ_R), the residence time of the H_2O molecule in the first coordination

sphere (τ_M) and the number of H_2O molecules directly bound to the central metal ion (q), all influence the inner-sphere contribution to the overall relaxivity. The effects of other parameters, such as the electronic relaxation rates ($T_{1e,2e}$) of the gadolinium(III) ion on this inner-sphere contribution [1][2][7] or of those parameters affecting the contribution of H_2O molecule(s) in the second hydration sphere [8] are much less understood.

The second hydration sphere, originating from H_2O molecules interacting with the complex but not directly bound to its metal ion [8], can significantly (5–15%) contribute to the overall relaxivity, particularly in complexes of P-containing ligands such as the Gd^{3+} complex of H_8DOTP (H_8DOTP = *P*,*P*′,*P*″,*P*‴-[1,4,7,10-tetraazacyclododecane-1,4,7,10-tetrayltetrakis(methylene)]tetrakis[phosphonic acid]) (*Fig. 1*). This complex does not contain a directly coordinated H_2O molecule [9] but its relaxivity r_1 is comparable to that of the clinically used $[Gd(H_2O)(DOTA)]^-$ complex (H_4DOTA = 1,4,7,10-tetraazacyclododecane-1,4,7,10-tetrayltetrakis[acetic acid] having one H_2O molecule in the first coordination sphere [10]. In the $[Gd(DOTP)]^{5-}$ complex, the H_2O-relaxation enhancement results exclusively from the second-sphere and outer-sphere (from H_2O molecules freely diffusing near the complex) contributions [11][12]. The H_8DOTP ligand and the series of $[Ln(DOTP)]^{5-}$ complexes have been extensively studied with regard to their crystal and solution structures and thermodynamic and relaxation properties [9–18]. Despite the promising *in vitro* relaxivity properties of the Gd^{3+} complex, highly charged complexes such as these are less desirable for *in vivo* use (the monoprotonated form $[Gd(HDOTP)]^{4-}$ predominates in solution at physiological pH) [18]. Since the $[Tm(HDOTP)]^{4-}$ complex binds efficiently to alkali-metal cations like Li^+, Na^+, or Cs^+ [16][18], it is also used as an alkali-metal NMR shift reagent in studies of isolated cells, tissues, and animals *in vivo* [19–23] as well as an extracellular *in vivo* tissue marker [24]. Again, accumulation of highly charged complexes such as this in bone will ultimately limit their use in humans [25].

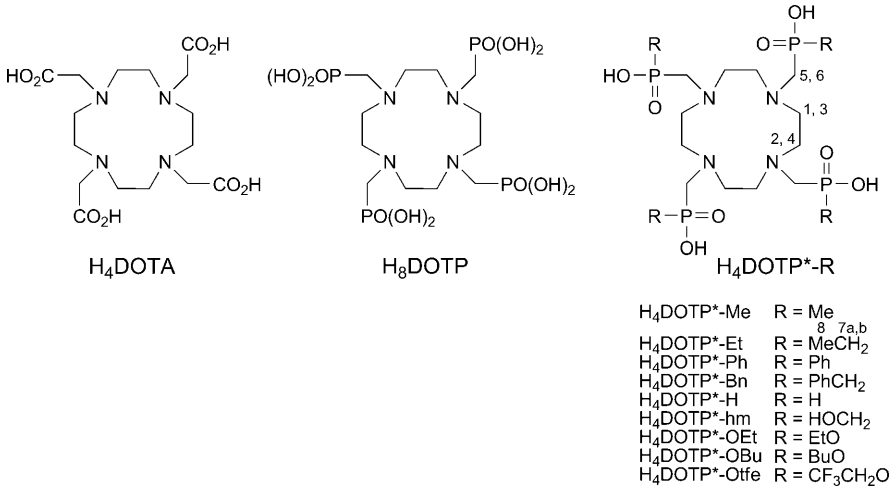

Fig. 1. *Chemical structures of the ligands mentioned in the text and the* (arbitrary) *proton-numbering scheme used in the* ^{1}*H-NMR study of the [Ln(DOTP*-Et)]*$^{5-}$ *complexes*

These results stimulated a search for new derivatives of this same basic structure which form Ln^{3+} complexes with differing charges and hydrophobicities. New DOTP-like Gd^{3+} complexes containing one hydrophobic substituent at the C-atom of one phosphonato side arm, such as octyl (C_8-DOTP), undecyl (C_{11}-DOTP), and *para*-nitrophenyl (NO_2-C_6H_4-DOTP), have increased *in vitro* relaxivities in the presence of human serum albumin (HSA) due to efficient binding to this blood protein [26]. The Gd^{3+} complexes of H_8DOTP-like ligands containing one substituent at all four phosphonic acid side arms, such as the tetraazatetrakisphosphonic acid *P*,*P*′,*P*″,*P*‴-tetraalkyl esters and the analogous phosphinic acid derivatives (see *Fig. 1* for some examples), have the advantage over $[Gd(DOTP)]^{5-}$ of having a single negative charge. A relaxometric study of the Gd^{3+} complexes of the related tetrakis[ethylphosphinic acid] ligand (H_4DOTP*-Et), and of the tetrakis[phosphonic acid] tetraethyl and tetrabutyl esters (H_4DOTP*-OEt = H_4DOTP-Et and H_4DOTP*-OBu = H_4DOTP-Bu, resp.) indicated only poor hydration (coordination number lower than one) [27]. The absence of directly coordinated H_2O molecules and the presence of second-sphere H_2O molecule(s) was also demonstrated for Gd^{3+} complexes of phosphinic acid ligands having methyl (H_4DOTP*-Me) [28], phenyl (H_4DOTP*-Ph) [29], or benzyl (H_4DOTP*-Bn) [30] substituents at the P-atom (*Fig. 1*). These second-sphere interactions are not much dependent on the structure of the complexes in solution [31].

In this work, we studied quantitatively the three-dimensional structure of the entire series of the Ln^{3+} complexes of one of such ligands, *P*,*P*′,*P*″,*P*‴-[1,4,7,10-tetraazacyclododecane-1,4,7,10-tetrayltetrakis(methylene)]tetrakis[ethylphosphinic acid] (H_4DOTP*-Et) (*Fig. 1*), *i.e.*, of the complexes $[Ln(DOTP*\text{-}Et)]^-$, in aqueous solution by means of ^{1}H-NMR, in particular by analyzing the paramagnetic shift and relaxation effects induced by the paramagnetic Ln^{3+} ions on the coordinated ligand nuclei. The published ^{31}P-NMR shifts for this series of complexes were also used in this analysis [31]. The results were compared with similar quantitative studies reported for the $[Ln(DOTP)]^{5-}$ complexes [16].

The complexity of the ^{1}H- and ^{31}P-NMR spectra precluded a similar quantitative comparison of the Ln^{3+} complexes of the tetraazatetrakisphosphonic acid ester ligands *P*,*P*′,*P*″,*P*‴-[1,4,7,10-tetraazacyclododecane-1,4,7,10-tetrayltetrakis(methylene)]tetrakis[phosphonic acid] tetraethyl ester (H_4DOTP*-OEt) ($\rightarrow [Ln(DOTP*\text{-}OEt)]^-$) and *P*,*P*′,*P*″,*P*‴-[1,4,7,10-tetraazacyclododecane-1,4,7,10-tetrayltetrakis(methylene)]tetrakis-[phosphonic acid] tetrabutyl ester (H_4DOTP*-OBu) ($\rightarrow [Ln(DOTP*\text{-}OBu)]^-$) (*Fig. 1*) [31], and only a qualitative structural analysis was undertaken. These were compared with published qualitative NMR studies on other phosphinato/phosphonato derivatives [29–32]. The effects of self-association and of various additives present in solution on their isomeric distribution was analyzed by ^{31}P-NMR, EPR, vapor-pressure osmometry, and luminescence spectroscopy.

2. Experimental. – *Materials and Methods.* All reagents and the lanthanide trichloride salts were obtained from commercial suppliers and used without further purification. The tetraazatetrakis[phosphonic acid] ligand H_8DOTP was obtained from *Macrocyclics* (Dallas, Texas, USA). The tetraazatetrakis[phosphonic acid] tetraalkyl esters H_4DOTP*-OEt and H_4DOTP*-OBu, and the tetraazatetrakis-[ethylphosphinic acid] ligand H_4DOTP*-Et were synthesized according to published procedures [27][31][33][34], and their purity was checked by ^{1}H- and ^{31}P-NMR. The simple phosphinic acid analog H_4DOTP*-H (= *P*,*P*′,*P*″,*P*‴-[1,4,7,10-tetraazacyclododecane-1,4,7,10-tetrayltetrakis(methylene)]tetrakis-

[phosphinic acid] (see *Fig. 1*), was kindly provided by Prof. *Ivan Lukeš* (Charles University of Prague, Czech Republic). The Ln^{3+} complexes of H_4DOTP*-Et, H_4DOTP*-OEt, H_4DOTP*-OBu, and H_4DOTP*-H were prepared as described before [31]. The aq. solns. of the Ln^{3+} complexes of H_8DOTP were prepared by mixing a 0.1M stock soln. of the ligand (10% excess) with the solid lanthanide triflates. The pH was adjusted to 10 with NaOH and, after stirring for 2 h, the pH, which dropped due to complex formation, was adjusted to 7.0. To check the absence of free Ln^{3+}, the xylenol-orange test [35] was performed for all the solutions.

NMR Measurements. High-resolution ^{1}H- and ^{31}P-NMR spectra: *Varian-Unity-500* (11.7 T) NMR spectrometer; at 499.82 and 202.33 MHz resp., with solns. of the complexes in D_2O (min 99.96% D, from *Aldrich Co.*) at 298 K. The pD of the solns. was adjusted with DCl or NaOD, and the pD values were estimated by adding 0.4 to the pH-meter readings. ^{1}H Shifts were referenced to TSP (sodium 3-(trimethylsilyl)(D_4)propanoate) as internal reference and ^{31}P shifts to 85% H_3PO_4 in H_2O as external reference. ^{1}H-NMR Spectra of the diamagnetic (La and Lu) and the two paramagnetic complexes (Eu and Nd) of $[Ln(DOTP*\text{-}Et)]^-$ were assigned by two-dimensional (2048 × 2048 data points in F_1 and F_2) COSY experiments. EXSY Spectra were obtained with a NOESY pulse sequence (10, 25, and 50 ms mixing time).

Analysis of LIS Data. The lanthanide-induced-shift (LIS) data were analyzed with the SHIFT ANALYSIS program developed by *Forsberg et al.* [36], where no assumption is made about the magnetic symmetry of the complex, by using as input data the Cartesian coordinates of the complexes with the lanthanide ion at the origin. The experimental pseudocontact LIS geometric factors (G) were fitted to calculated values for various isomeric structures by means of the components of the susceptibility tensor as adjustable parameters: When only fragments of these structures were used, axial symmetry of the shifts was assumed. Averaging of G values of symmetry-related resonances was not carried out prior to the comparison with the experimental values. The agreement between the observed and calculated values was evaluated with *Hamilton*'s crystallographic agreement factor [37] defined as $AF_j = [\Sigma_j (\delta_{ij}^{exp} - \delta_{ij}^{calc})^2]/\Sigma_j (\delta_{ij}^{exp})^2]^{1/2}$, where δ_{ij}^{exp} and δ_{ij}^{calc} represent the observed and calculated shift values of a nucleus i in a given Ln^{3+} complex j, resp.

EPR Measurements. Electron paramagnetic resonance measurements were carried out with a *Bruker-ESP-300E* spectrometer, operating at 9.34 GHz (0.34 T, X-band). The EPR spectra of the $[Gd(DOTP*\text{-}H)]^-$, $[Gd(DOTP*\text{-}Et)]^-$, $[Gd(DOTP*\text{-}OEt)]^-$, and $[Gd(DOTP*\text{-}OBu)]^-$ complexes were measured in aq. solns. at pH 7.0 and 298 K in the 1 – 10 mM concentration range with a quartz flat cell. Typical parameters used for spectral acquisition were: sweep width 40 mT, microwave power in the 0.632 mW range, modulation amplitude 0.32 mT, time constant 20.48 ms.

Vapor-Pressure Osmometry. The osmolality of solutions of H_8DOTP, H_4DOTP*-Et, $[Eu(DOTP)]^{5-}$, and $[Eu(DOTP*\text{-}Et)]^-$, between 2.5 and 50 mM were measured with a *Wescor-5500* vapor-pressure osmometer at room temperature, pH 7.

Luminescence Spectroscopy. Luminescence measurements were performed with a *Fluorolog-2* spectrofluorimeter and a 450 W Xe lamp for excitation at 355 nm. Luminescence emission of $[Tb(DOTP*\text{-}Et)]^-$ in aq. soln. (pH 7) was measured at 544 nm in the absence and the presence of increasing concentrations of $[Eu(DOTP*\text{-}Et)]^-$. Each sample was purged with N_2 gas for 5 min before measurement.

Computations. Molecular mechanics was performed with HyperChem (version 7.5, MM+ force field, *HyperCube Inc.*, Gainsville, FI).

3. Results and Discussion. – 3.1. *Stabilities of the Studied Complexes.* The protonation constants of the H_4DOTP*-Et, H_4DOTP*-OBu and other similar ligands, as well as the stability constants of the corresponding Gd^{3+} complexes were determined previously by pH potentiometry [31][33][34]. The values of the stability constants show that the $[Gd(DOTP*\text{-}OBu)]^-$ complex ($\log K_{GdL} = 12.19$) [33] is less stable than $[Gd(DOTP*\text{-}Et)]^-$ ($\log K_{GdL} = 16.50$) [34], and both are much less stable than $[Gd(DOTP)]^{5-}$ ($\log K_{GdL} = 28.8$) [18]. These differences reflect the charge of the ligands and the basicity of the ligand donor atoms [13][14].

3.2. *NMR Structure of [Ln(DOTP*-Et)]*$^{-}$. The structures of complexes of the tetraazatetrakis[phosphinato/phosphonato] derivatives are generally analogous to those of complexes of H_4DOTA, where the Ln^{3+} ion is situated between the N_4- and O_4-planes. The H_4DOTA complexes are present in solution in two diastereoisomeric forms differing in the mutual rotation of the N_4- and O_4-planes, giving a square-antiprismatic arrangement (SA; torsion angle $\theta > 35°$, with opposite sign of rotation of the pendant arms (Δ/Λ) and the conformation of the ethane-1,2-diyl moieties in the macrocycle ring (δ/λ), represented as the $\Delta\lambda\lambda\lambda\lambda/\Lambda\delta\delta\delta\delta$ isomeric pair, traditionally termed '**M**') and a twisted-square-antiprismatic arrangement (TSA; torsion angle $\theta < 30°$, with the same sign of rotation leading to the $\Lambda\lambda\lambda\lambda/\Delta\delta\delta\delta$ pair, traditionally termed '**m**') [38]. However, the Ln^{3+} complexes of the alkyl-DOTP* (phosphinato) or alkoxy-DOTP* (phosphonato ester) ligands occur exclusively in the **m** conformation ($\Lambda\lambda\lambda\lambda/\Delta\delta\delta\delta$), possibly due to the more demanding stereochemical requirements of the phosphi(o)-nato chelating groups and the bulky pendant arms [9][16][29][30]. Then, as a result of the four extra stereogenic centers due to the chirality of the P-atoms in these complexes, in principle 32 stereoisomers are possible, existing as 16 NMR-indistinguishable enantiomer pairs. For the remainder of this article, we will refer only to the chirality of the P-atoms in the $\Delta\delta\delta\delta$ configuration; for example (*R*,*R*,*R*,*R*) refers to the NMR-indistinguishable pair of enantiomers $\Delta\delta\delta\delta$-(*R*,*R*,*R*,*R*)/$\Lambda\lambda\lambda\lambda$-(*S*,*S*,*S*,*S*). In complexes with equal pendant arms, the number of possible diastereoisomers is further reduced to six: (*R*,*R*,*R*,*R*), (*R*,*R*,*R*,*S*), (*R*,*R*,*S*,*S*), (*R*,*S*,*R*,*S*), (*S*,*S*,*S*,*R*), and (*S*,*S*,*S*,*S*). These species have the relative statistical abundances 1:4:4:2:4:1. The different diastereoisomers have different shapes and energies, as shown by molecular-mechanics calculations for the [Ln(DOTP*-Otfe)]$^{-}$ complexes ($R = CF_3CH_2$ in *Fig. 1*) [32].

3.3. *NMR Spectra.* To obtain structural information on the [Ln(DOTP*-Et)]$^{-}$ complexes in solution, ^{1}H- and ^{31}P-NMR spectra were acquired for the whole lanthanide series (except for Pm and Gd). The diamagnetic [Ln(DOTP*-Et)]$^{-}$ (Ln = La, Lu) complexes exhibit ^{1}H-NMR spectra with eight (La) or seven (Lu) *m* (*Fig. S1* in the Supplementary Material[1])), possibly corresponding to a single symmetrical isomer (*R*,*R*,*R*,*R*) or (*S*,*S*,*S*,*S*), although the presence of other isomers with very small differences in diamagnetic chemical shifts cannot be excluded. The spectrum of the Lu^{3+} complex is significantly sharper, suggesting a higher internal rigidity. The assignments were based upon literature data from similar systems [16][32] and COSY plots, which showed vicinal couplings between H(1)/H(4), H(2)/H(3), H(8)/H(7a) and H(8)/H(7b) pairs, and geminal couplings between the pairs H(1)/H(3), H(2)/H(4), H(5)/H(6), and H(7a)/H(7b) for both diamagnetic complexes (data not shown) (for atom numbering, see *Fig. 1*). The ^{31}P-NMR spectra of the diamagnetic La^{3+} and Lu^{3+} complexes were also obtained (*Fig. 2*). These spectra are quite simple, showing one dominant major signal, corresponding to the four equivalent phosphinato P-atoms of the C_4-symmetric (*R*,*R*,*R*,*R*) (or (*S*,*S*,*S*,*S*)) isomer, but also several minor signals resulting from one minor isomer.

These results were confirmed by the ^{1}H- and ^{31}P-NMR spectra of the whole series of paramagnetic [Ln(DOTP*-Et]$^{-}$ complexes (Ln = Ce – Yb, except for Pm and Gd). All the ^{31}P-NMR spectra show the dominant major and minor signals, which vary in shift

[1]) The supplementary material may be obtained upon request from the authors.

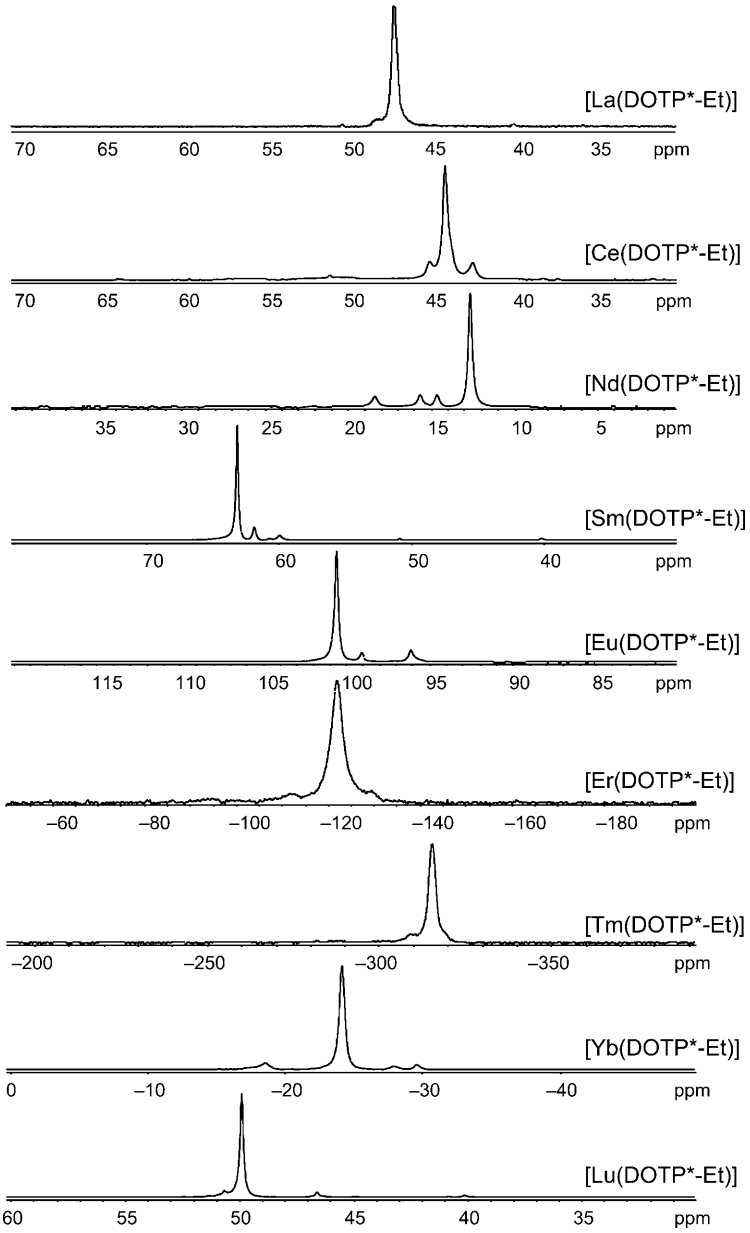

Fig. 2. *^{31}P-NMR Spectra of some [Ln(DOTP*-Et)]$^{-}$ complexes* (Ln = Ce, Nd, Sm, Eu, Er, Tm, Yb, and Lu; 10 mM, pH 7.0, 298 K, D_2O)

magnitude and intensity according to the lanthanide complex (*Fig. 2*). In these spectra, the minor resonances could be assigned to the asymmetric (*R*,*R*,*R*,*S*) (or (*S*,*S*,*S*,*R*)) isomer, which gives four signals for the nonequivalent P-atoms, not all of which are

always visible. The population of the major isomer, calculated from the intensities of the NMR signals, varies between 80 and 84% along the lanthanide series [31]. The chemical exchange between the major and minor isomers could be demonstrated by the presence of exchange cross-peaks of the two-dimensional exchange (EXSY) spectrum, *e.g.*, for the $[Nd(DOTP^*\text{-}Et)]^-$ complex (*Fig. S2*)[1]). The intensity of these cross-peaks reaches a maximum at a contact time of around 25 ms.

The ^{1}H-NMR spectra, illustrated in *Fig. 3* for the Pr^{3+} and Eu^{3+} complexes, were assigned on the basis of COSY plots for the Ce to Eu complexes and also by comparison with the shifts of H(1) to H(6) of the corresponding $[Ln(DOTP)]^{5-}$ complexes [16]. The spectrum of the Eu^{3+} complex has one resonance from the macrocyclic axial proton H(4) at δ 32 (see *Fig. 1* for atom numbering and *Table S1*)[1]), characteristic of the exclusive presence of the TSA isomeric structure. All the spectra show the presence of the dominant C_4-symmetric (*R*,*R*,*R*,*R*) (or (*S*,*S*,*S*,*S*)) isomer and very small amounts of the asymmetric (*R*,*R*,*R*,*S*) (or (*S*,*S*,*S*,*R*)) isomer, in agreement with the ^{31}P-NMR spectra [31]. The dominance of the symmetric isomer is ascribed to the strong preference for the same type of arrangement around neighboring P-atoms, (*R*,*R*) (or (*S*,*S*)) relative to the (*R*,*S*) (or (*S*,*R*)) orientation, as the steric hindrance between those substituent groups and the electronic repulsions between the partially charged O-atoms is higher in the (*R*,*S*) orientation [32].

Several studies of other DOTP*-like phosphinato derivatives have been reported, both in the solid state and in solution [31][32]. In the crystal structures of $[Ln(DOTP^*\text{-}Bn)]^-$ ($R = PhCH_2$, $H_4DOTP^*\text{-}Bn$ = *P*,*P*′,*P*″,*P*‴-[1,4,7,10-tetraazacyclododecane-1,4,7,10-tetrayltetrakis(methylene)]tetrakis[benzylphosphinic acid) [30a] and $[Ln(DOTP^*\text{-}Me)]^-$ ($R = Me$, $H_4DOTP^*\text{-}Me$ = *P*,*P*′,*P*″,*P*‴-[1,4,7,10-tetraazacyclododecane-1,4,7,10-tetrayltetrakis(methylene)]tetrakis[methylphosphinic acid]) (*Fig. 1*) [30c], only the (*R*,*R*,*R*,*R*) ((*S*,*S*,*S*,*S*)) diastereoisomer was found in the solid state, while for the $[Ln(DOTP^*\text{-}Ph)]^-$ ($R = Ph$, $H_4DOTP^*\text{-}Ph$ = *P*,*P*′,*P*″,*P*‴-[1,4,7,10-tetraazacyclododecane-1,4,7,10-tetrayltetrakis(methylene)]tetrakis[phenylphosphinic acid]), $[Gd(DOTP^*\text{-}H)]^-$, and $[Gd(DOTP^*\text{-}OEt)]^-$ complexes, the phosphi(o)nato groups are orientated according to the (*R*,*S*,*R*,*S*) diastereoisomer with alternating absolute configurations of the pendant arms [29][31]. All the crystal structures confirm the exclusive presence of the TSA isomer.

In aqueous solution, various diastereoisomers were found in all cases. For the $[Ln(DOTP^*\text{-}Bn)]^-$, $[Ln(DOTP^*\text{-}Me)]^-$, and $[Ln(DOTP^*\text{-}hm)]^-$ ($R = HOCH_2$, *Fig. 1*) complexes, the (*R*,*R*,*R*,*R*) (or (*S*,*S*,*S*,*S*)) form was always dominant, but their absolute configuration could not be obtained [30b][31]. The latter complex is quite similar to the $[Ln(DOTP^*\text{-}Et)]^-$ complexes studied here, with similar results. In the case of the $[Ln(DOTP^*\text{-}Ph)]^-$ complexes, that dominance did not occur, and the following relative population order was obtained: (*R*,*R*,*R*,*S*) > (*R*,*R*,*R*,*R*) > (*R*,*R*,*S*,*S*) > (*R*,*S*,*R*,*S*) > (*R*,*S*,*S*,*S*) > (*S*,*S*,*S*,*S*) [29]. The presence of complex diastereoisomer mixtures in solution was also concluded for the $[Ln(DOTP^*\text{-}H)]^-$, $[Gd(DOTP^*\text{-}OEt)]^-$, and $[Ln(DOTP^*\text{-}OBu)]^-$ complexes from their ^{31}P-NMR spectra [31]. In the case of the $[Ln(DOTP^*\text{-}Otfe)]^-$ complexes (Ln = Dy, Tm, and Yb), a combined ^{19}F- and ^{31}P-NMR study has shown that all diastereoisomers are present, with the relative population order (*R*,*R*,*R*,*R*) ≈ (*S*,*S*,*S*,*S*) > (*R*,*R*,*R*,*S*) ≈ (*R*,*R*,*S*,*S*) ≈ (*R*,*S*,*S*,*S*) > (*R*,*S*,*R*,*S*) [32]. This shows that the way in which the steric

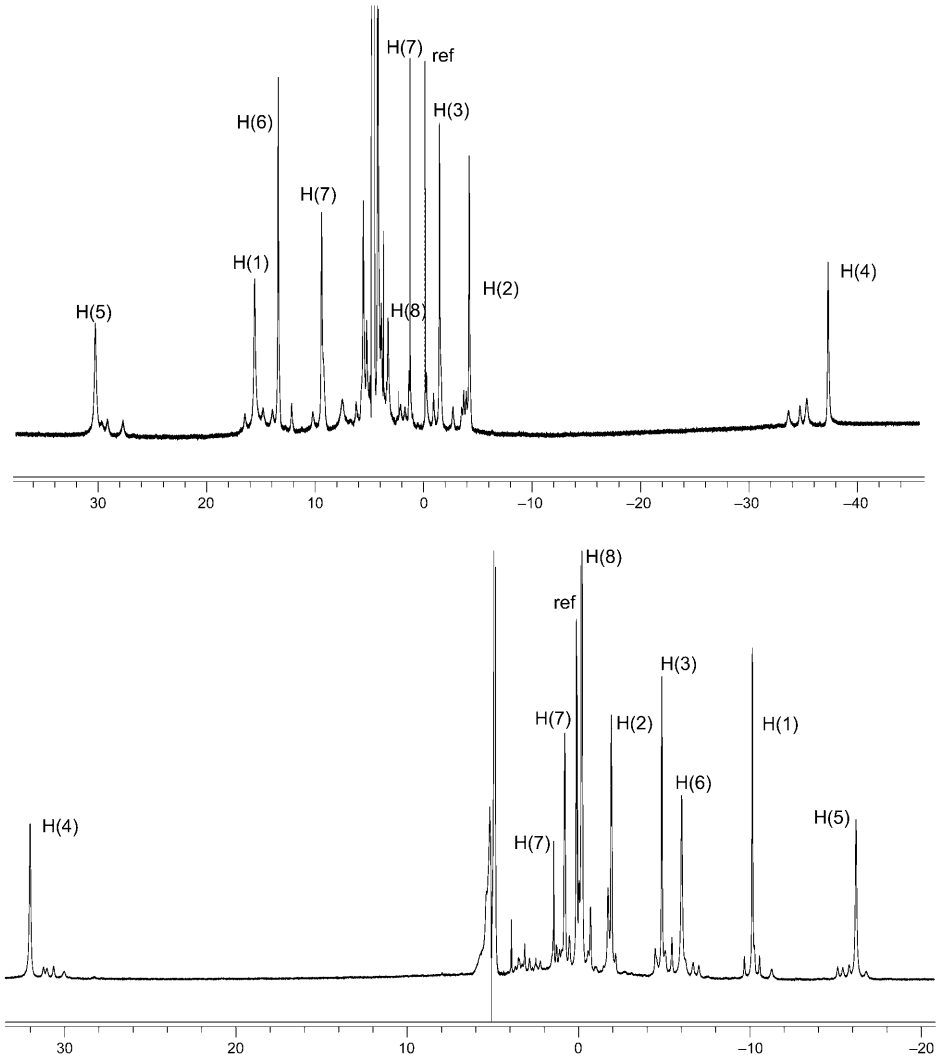

Fig. 3. *^{1}H-NMR Spectra of some [Ln(DOTP*-Et)]$^-$ complexes* (10 mM, pH 7.0, 298 K, D_2O). Top, Ln = Pr; bottom, Ln = Eu. See *Fig. 1* for atom numbering.

demands of the substituent groups affect the relative diastereoisomer populations in the various complexes is not obvious.

A summary of the ^{1}H and ^{31}P lanthanide-induced shifts (LIS) obtained for the dominant C_4-symmetric (*R*,*R*,*R*,*R*) (or (*S*,*S*,*S*,*S*)) isomer of the [Ln(DOTP*-Et)]$^-$ complexes is given in the supplementary material (*Table S1*, pH 7.0 and 298 K)[1]). The resonances of the other nonsymmetric isomer could not be specifically assigned. All the LIS values were measured relative to the La complex for the first part of the series (Ce to Eu) and relative to the Lu complex for the second part of the series (Tb to Yb).

3.4. *Separation of Contact and Pseudocontact Shift Contributions.* For a given nucleus i in a Ln^{3+} paramagnetic complex, the lanthanide-induced shift (Δ_i) consists of three contributions [39], diamagnetic (Δ_i^d), contact (Δ_i^c), and pseudocontact (Δ_i^{pc}) or dipolar (*Eqn. 1*).

$$\Delta_i = \Delta_i^d + \Delta_i^c + \Delta_i^{pc} \tag{1}$$

Diamagnetic shifts originate from conformational changes, inductive effects and/or direct field effects and can be determined from the shifts induced by the diamagnetic members of the series (La^{3+} and Lu^{3+}), as described above. The contact contribution, Δ_i^c originates from a through-bond transmission of unpaired spin density of Ln^{3+} to the ligands, and the pseudocontact (Δ_i^{pc}) results from a through-space dipolar interaction between the magnetic moments of the unpaired electrons in Ln^{3+} and the ligand nucleus [39].

Upon subtracting the diamagnetic contribution, the pure paramagnetic contribution for nucleus i, Δ'_i, is obtained , which can be expressed by *Eqn. 2*, where $\langle S_z \rangle_j$ and C_j^D, the spin expectation values and the magnetic constant of the Ln^{3+} ions, respectively, are characteristic of the ions but independent of the ligand, while F_i is proportional to the scalar hyperfine coupling constant between the unpaired spin density of the lanthanide ion j and the nucleus i of the ligand under study, and $G_i = G_{i1} \langle r^2 \rangle A_2^0 + G_{i2} \langle r^2 \rangle A_2^2$ is a combination of the ligand-field coefficients A_2^0 and A_2^2 with the geometric factors, $G_{i1} = (3\cos^2\theta - 1)/r^3$ and $G_{i2} = (\sin^2\theta \cos^2\varphi)/r^3$, of the nucleus, which contain the structural information about the complex through the spherical coordinates r, θ, and φ of the observed nucleus with respect to the Ln^{3+} at the origin. The dipolar contribution can be rewritten in the form of *Eqn. 3* where the constants D_1 and D_2 are proportional, respectively, to the axial ($\chi_{zz} - 1/3(\chi_{xx} + \chi_{yy} + \chi_{zz})$) and rhombic ($\chi_{xx} - \chi_{yy}$) anisotropies of the magnetic susceptibility tensor χ. In the special case of axial symmetry, the second term of *Eqn. 3* vanishes since $D_2 = 0$.

$$\Delta'_i = \Delta_i^c + \Delta_i^{pc} = \langle S_z \rangle_j F_i + C_j^D G_i \tag{2}$$

$$\Delta_i^{pc} = D_1 (3\cos^2\theta - 1)/r^3 + D_2 (\sin^2\theta \cos^2\varphi)/r^3 \tag{3}$$

The contact and pseudocontact contributions can be separated according to a structure-independent method [40], based on the rearrangement of *Eqn. 2* into the two linear forms of *Eqns. 4* and *5*.

$$\Delta'_i/\langle S_z \rangle_j = F_i + (C_j^D/\langle S_z \rangle_j) G_i \tag{4}$$

$$\Delta'_i/C_j^D = (\langle S_z \rangle_j / C_j^D) F_i + G_i \tag{5}$$

When a series of lanthanide complexes is isostructural, the F_i and G_i values for the ligand are independent of the lanthanide ion, and plots according to *Eqns. 4* and *5* are straight lines. The F_i and G_i terms can then be determined as the slope and intercept in

the plots according to *Eqn. 4*, or *vice versa* in the plots according to *Eqn. 5*. The first equation is used to study nuclei with a predominant pseudocontact contribution, such as a proton or a ^{31}P-nucleus relatively far away from the Ln^{3+} ion, while the second is used to examine nuclei with a predominant contact shift, such as ^{17}O in a H_2O molecule directly coordinated to the Ln^{3+} ion. When slight changes in the orientation of the ligand around the lanthanide ion occur, this difference is reflected in small changes of *G*. However, *F* values are not affected by these slight structural changes, and plots according to *Eqn. 5* continue to be straight lines. When a significant structural change occurs across the lanthanide series, neither *F* nor *G* are constants and both plots are nonlinear, showing a break [39].

The contact and pseudocontact contributions to the observed LIS values for the (*R*,*R*,*R*,*R*) (or (*S*,*S*,*S*,*S*)) isomer of the $[Ln(DOTP^*\text{-Et})]^-$ series of complexes were separated by means of *Eqns. 4* and *5*. The corresponding plots for H(1) and H(5) are shown in *Fig. 4*, and the plots for all nuclei studied can be seen in *Figs. S3* and *S4*[1]). The same plots for the ^{31}P-nucleus have been published before [31]. Most plots according to *Eqn. 4* show a break between the early (Ce → Eu) and late (Tb → Yb) lanthanide half-series. Plots according to *Eqn. 5* show some scatter in the data, perhaps due to the low contact contribution in the LIS values of these nuclei. Such breaks have also been observed for the ^{31}P LIS values of the $[Ln(DOTP^*\text{-Bn})]^-$ complexes [30a] where it was attributed to a change of inner-sphere H_2O coordination from $q = 1$ for (Ce → Nd) to $q = 0$ for (Eu → Yb). The $[Ln(DOTP^*\text{-Ph})]^-$ complexes did not show such a break and were, thus, considered to be isostructural, with a hydration number $q = 0$ all along the lanthanide series [29]. However, these conclusions must be taken with care. It has recently been shown, for the predominant (*R*,*R*,*R*,*R*) ((*S*,*S*,*S*,*S*)) solution isomer of the series of complexes $[Ln(DOTP^*\text{-H})]^-$, $[Ln(DOTP^*\text{-hm})]^-$, $[Ln(DOTP^*\text{-OEt})]^-$, and $[Ln(H_{1.5}DOTP)]^{3.5-}$, that the positions of the breaks observed in the plots of the H_2O ^{17}O LIS values, which directly reflect the change of inner-sphere H_2O coordination, do not correspond with those observed for the ^{31}P LIS data [31]. These latter breaks, observed at the middle of the Ln series, indicate a change in both *F* and *G* for the ^{31}P-nucleus of these complexes along the series, reflecting a geometric change in the TSA coordination sphere, whereby the Ln^{3+} ion inside the ligand cavity moves towards the N_4-plane upon going from La to Eu, after which it remains at a nearly constant position for the rest of the series [31][41][42]. However, in those systems, the ^{17}O LIS values have shown that $q = 0$ along the whole series, with the exception of some cases of Ce^{3+} complexes with $q = 1$. Thus the ^{1}H and ^{31}P LIS breaks may not directly reflect a change of hydration number of the complex, and most of the $[Ln(DOTP^*\text{-Et})]^-$ complexes (with the possible exception of those at the beginning of the series, like Ce^{3+}) should have $q = 0$, like the Gd^{3+} complex, as shown from the interpretation of its NMRD profiles [31].

Tables 1 and *S2*[1]) show the values of *F* and *G* obtained from the linear least-squares analysis of the LIS data according to *Eqns. 4* and *5*, respectively, by separating the data into two subgroups of lanthanide cations, Ce → Eu (removing Sm) and Tb → Yb (removing Tm), and for the entire series, Ce → Eu (removing Sm and Tm), as the Sm and Tm shifts were often completely out of the linear trends defined by the other data.

3.5. *Comparison of the Experimental and Calculated LIS Values.* The analysis of the pseudocontact shifts to obtain structural information is initiated by assuming some

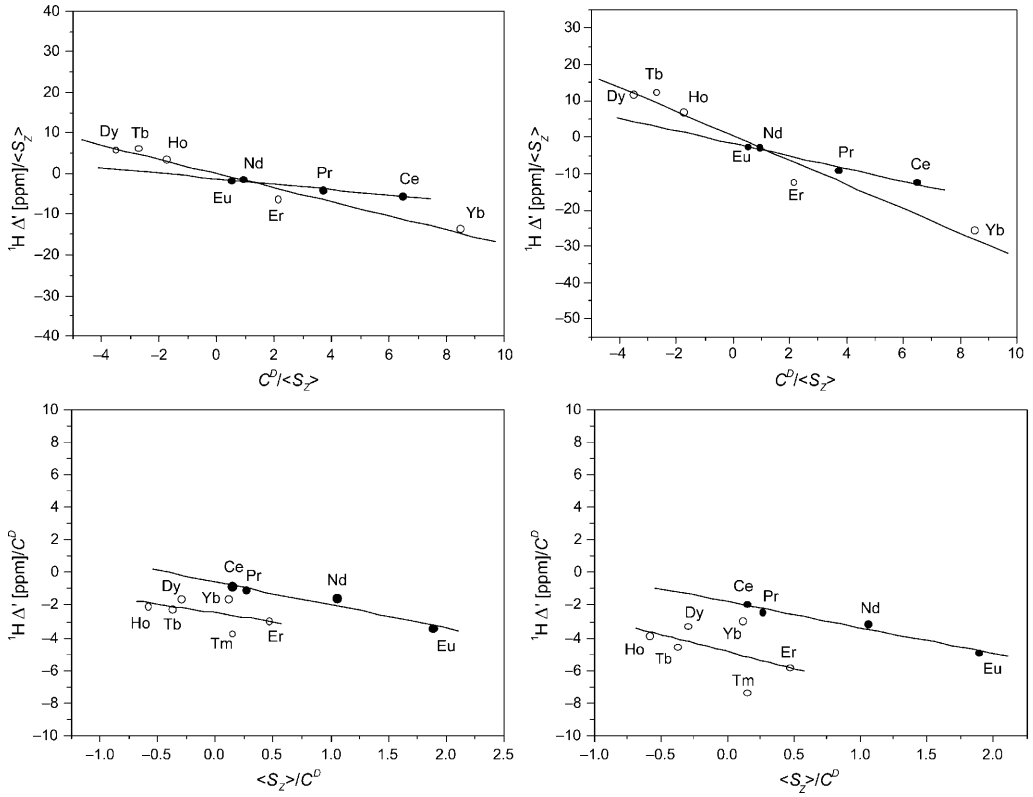

Fig. 4. *Plots of the separation of contact and pseudocontact contributions to the LIS data of protons H(1)* (left) *and H(5)* (right) *according to* Eqn. 4 (top) *and* Eqn. 5 (bottom) *for the (*R,R,R,R*)* (or (*S,S,S,S*)) *isomer of [Ln(DOTP*-Et)]*$^{-}$ *complexes*

Table 1. *Separation of Contact and Pseudocontact Contribution to the Observed LIS in the Paramagnetic (*R,R,R,R) (or (*S,S,S,S*)) *Isomer of [Ln(DOTP*-Et)]*$^{-}$ *Complexes According to* Eqn. 4 (errors in parenthesis)

	Ce → Eu (– Sm)		Tb → Yb (– Tm)		Ce → Yb (– Sm and Tm)	
	F	*G*	*F*	*G*	*F*	*G*
H(1)	– 1.3 (0.3)	– 0.7 (0.1)	0.0 (0.8)	– 1.7 (0.2)	0.4 (0.8)	– 1.5 (0.2)
H(2)	– 1.4 (0.5)	0.8 (0.2)	0.2 (1.1)	1.1 (0.2)	– 0.9 (0.4)	0.8 (0.1)
H(3)	– 1.3 (0.2)	0.6 (0.1)	0.5 (1.1)	0.8 (0.2)	– 0.5 (0.6)	0.6 (0.1)
H(4)	2.4 (0.7)	2.8 (0.1)	1.2 (2.0)	4.4 (0.5)	0.3 (1.5)	4.0 (0.4)
H(5)	– 1.7 (0.6)	– 1.8 (0.1)	0.3 (1.8)	– 3.3 (0.4)	0.9 (1.4)	– 3.0 (0.3)
H(6)	– 1.1 (0.4)	– 0.6 (0.1)	– 0.4 (0.7)	– 1.3 (0.2)	0.0 (0.6)	– 1.1 (0.2)
H(7a)	0.2 (0.2)	– 0.7 (0.1)	– 0.7 (1.1)	– 0.3 (0.2)	– 0.5 (0.5)	– 0.2 (0.1)
H(7b)	0.7 (0.4)	– 0.3 (0.1)	0.9 (0.4)	– 0.3 (0.1)	0.7 (0.2)	– 0.4 (0.1)
H(8)	0.4 (0.26)	– 0.4 (0.1)	0.1 (0.2)	– 0.2 (0.0)	0.0 (0.1)	– 0.2 (0.0)
^{31}P	7.5 (1.4)	– 0.9 (0.7)	1.9 (1.7)	– 3.8 (0.4)	6.5 (3.2)	– 2.8 (0.8)

structure for the complex in solution, thereby allowing the calculation of the geometric factors. Firstly, for the comparison between the experimental ^{1}H and ^{31}P pseudocontact LIS values of the $[Ln(DOTP^{*}\text{-}Et)]^{-}$ complexes, taken as the experimentally obtained geometric terms of nucleus i (G_i values) of *Table 1*, with the corresponding calculated values obtained with the SHIFT ANALYSIS program [36], several geometric models were considered. For each model, the atomic coordinates of the H- and P-atoms of the complex with the Ln^{3+} fixed at the origin of the system were used as input to the calculation. The atomic coordinates were obtained from those of the crystal structure of the $[Gd(DOTP^{*}\text{-}OEt)]^{-}$ complex [31]. In this structure, the Gd^{3+} ion is octacoordinated by four macrocyclic N-atoms and four O-atoms of the pendant arms, forming two parallel N_4 and O_4 planes, with twisted square antiprismatic (TSAP, $\Lambda\lambda\lambda\lambda/\Delta\delta\delta\delta$) coordination geometries with torsion angles between the N_4 and O_4 planes of *ca.* -28°. As the absolute configuration of the four phosphonato monoester side chains in this structure is (S,R,S,R), they were modified to assume (R,R,R,R) and (S,S,S,S) structures by means of the HyperChem program, followed by a geometry optimization on these modified arms and keeping the (S,S,S,S) and (R,R,R,R) diastereoisomers in the initial TSAP geometry. This structure, with $q = 0$, is a good starting model for the structure of the complexes of the second half of the Ln series, and probably also for most of the first half, as discussed above. The calculated LIS values for the side chain CH_2 and Me protons were averaged, simulating free rotation of their P–C–C bonds. The four chemically equivalent fragments around each N-atom and phosphinato group in the $[Gd(DOTP^{*}\text{-}Et)]^{-}$ molecular model constructed as described above do not have exactly equivalent conformations, due to small distortions of the crystal structure of the parent $[Gd(DOTP^{*}\text{-}OEt)]^{-}$ complex. When all the ^{1}H and ^{31}P nuclei of the model were initially used simultaneously in the calculations, the magnetic symmetry of the complex was assumed to be rhombic, and equal weights were used for all LIS values when running the least-squares analysis in the SHIFT ANALYSIS program. In this case, the calculated values of the main components of the magnetic susceptibility tensor (χ) should tell how close the complex is to true axial symmetry. Similar calculations were also carried out by using separately the ^{1}H and ^{31}P nuclei of each of the four fragments of the $[Gd(DOTP^{*}\text{-}Et)]^{-}$ model.

The agreement between the calculated shifts and the experimental G_i values was very poor in all cases considered: for the (R,R,R,R) conformation, $AF_j \geq 0.7182$ values were obtained for the first and second half of the lanthanide series with either *Eqn. 4* or *5*, which decreased to still rather poor AF_j values ≥ 0.4920 for the best of the four molecular fragments used. When the same calculations were carried out for the (S,S,S,S) conformation, equally poor results were obtained: $AF_j \geq 0.7909$ using all the nuclei, and $AF_j \geq 0.3151$ for the best molecular fragment. Possibly, the poor agreement can be ascribed to the inadequacy of the shift-separation method in the present case due to structural changes that occur across the lanthanide series.

Therefore, new calculations were performed with the experimental ^{1}H and ^{31}P LIS values of a single lanthanide complex, $[Yb(DOTP^{*}\text{-}Et)]^{-}$ (*Table S1*[1]). It was assumed that these LIS values are exclusively of pseudocontact origin, which is usually a good approximation [32][39]. The calculations were performed separately for each of the four equivalent fragments, and the LIS values for the Me protons (H(8)) were not considered in the fitting procedure, due to the averaging effect of the mobility of the

pendant arms on their LIS values. The best fits obtained for the (*R*,*R*,*R*,*R*) and (*S*,*S*,*S*,*S*) isomers are shown in *Table 2*. The LIS values of the [Yb(DOTP*-Et)]$^-$ complex were better fitted for the (*R*,*R*,*R*,*R*) isomer ($AF_j = 0.071$) than for the (*S*,*S*,*S*,*S*) isomer ($AF_j = 0.175$). The negative sign of the experimental G_i values obtained for H(7) and H(8) protons of the Et chains, which is the same as for the methylene protons H(5) and H(6) (*Table 1*), as well as the negative LIS values observed for the H(7b) and H(8) protons of [Yb(DOTP*-Et)]$^-$ (*Table 2*), indicate that the major isomer has a (*R*,*R*,*R*,*R*) configuration, as the (*S*,*S*,*S*,*S*) isomer would have those chains concentrated on the positive rather than the negative side of the dipolar cone. However, this conclusion should be taken with caution, as motional averaging of the side chains might significantly change the geometric factors of those protons.

Table 2. *Comparison of Observed*[a]) *and Calculated*[b]) *Proton Pseudocontact LIS Values for the Paramagnetic [Yb(DOTP*-Et)]$^-$ Complex* (standard deviations for the shifts in parenthesis)

	(*R*,*R*,*R*,*R*) Isomer		(*S*,*S*,*S*,*S*) Isomer	
	LIS_{exp}	LIS_{calc}	LIS_{exp}	LIS_{calc}
H(1)	−35.4	−34.4 (4.5)	−35.4	−12.5 (41.1)
H(2)	16.3	15.4 (4.4)	16.4	3.2 (20.4)
H(3)	11.9	14.1 (1.8)	11.9	22.5 (20.8)
H(4)	92.4	94.1 (8.5)	92.4	91.0 (28.3)
H(5)	−66.5	−75.1 (3.2)	−66.5	−63.3 (34.9)
H(6)	−27.9	1.0 (12.3)	−27.9	0.2 (18.9)
H(7a)	0.6	−0.4 (10.4)	0.6	20.6 (7.0)
H(7b)	−7.9	12.6 (5.54)	−7.9	30.1 (8.5)
H(8)[c])	−2.0	–	−2.0	–
^{31}P	−74.0	−63.2 (5.4)	−74.0	−54.9 (41.1)

[a]) The observed proton pseudocontact LIS values are taken as the experimentally observed LIS values of *Table S1*[1]) for the Yb^{3+} complex. [b]) Values calculated with the program SHIFT ANALYSIS and by side-chain modification of the crystal coordinates of the [Gd(DOTP*-OEt)]$^-$ complex. $AF = 0.071$ ((*R*,*R*,*R*,*R*) isomer) and $AF = 0.175$ ((*S*,*S*,*S*,*S*) isomer). [c]) The corresponding protons were not considered during the calculations.

3.6. *Self-Association of the Complexes and Effects of Detergents.* 3.6.1. *Preamble.* The self-association of some tetraazatetrakis[phosphi(o)nato] complexes, [Ln(DOTP*-Et)]$^-$, [Ln(DOTP*-OEt)]$^-$, [Ln(DOTP*-OBu)]$^-$, [Ln(DOTP*-H)]$^-$, and [Ln(DOTP)]$^{5-}$, in aqueous solution was studied by a combination of techniques, including NMR, EPR, osmolality, and luminescence measurements. It has been observed by gel filtration that [Gd(DOTP)]$^{5-}$ self-associates in aqueous solutions under certain conditions [10], and there is NMR evidence for intermolecular interactions for [Ln(DOTP*-Otfe)]$^-$ complexes [32]. Complexes that show a complex isomer mixture in solution were chosen to detect any change of this distribution as a consequence of their intermolecular interactions (self-association and/or effect of detergents).

3.6.2. *^{31}P-NMR Studies.* The ^{31}P-NMR spectra of the [Ln(DOTP*-OBu)]$^-$ complexes, both diamagnetic (Ln = Lu) and paramagnetic ones (Ln = Ce – Yb, except for Pm and Gd), show a large number of signals, clearly indicating the presence of

isomer mixtures in solution (*Fig. S5*[1])) [31]. The same complexity was observed for the ^{1}H-NMR spectra (*Figs. S6* and *S7*[1])). Each P-atom produces a variety of signals, which could not be specifically assigned to the possible diastereoisomers resulting from the (*R*) or (*S*) configurations at each P-atom. The ^{31}P-NMR spectra of [Ln(DOTP*-OEt)]$^-$, and [Ln(DOTP*-H)]$^-$ also show the presence of big isomer mixtures in solution [31].

The ^{31}P-NMR spectra of [Eu(DOTP*-OBu)]$^-$ (*Fig. 5*) and [Eu(DOTP*-OEt)]$^-$ (*Fig. S8*[1])) complexes were obtained in the concentration range 0.1–20 (or 25) mM since self-association has been observed previously in DOTP-like Ln^{3+} complexes [10]. The spectra of [Eu(DOTP*-OBu)]$^-$ show a significant change of the isomer-mixture composition when the concentration is increased, as shown by the changes of relative intensities and shifts of the resonances in the shift range δ 47–53, in particular the one at δ 51. The ^{31}P-NMR spectra of [Eu(DOTP*-OEt)]$^-$ also show a concentration dependence of the peak intensities and shifts, and extensive broadening and overlap is observed at concentrations at and above 5 mM. Also, a very broad peak appears at δ *ca.* 30 (10 mM) which is shifted to δ *ca.* 5 for the 25 mM solutions. This indicates the presence of extensive self-association of the complexes at and above 5 mM.

The effect of the addition of surfactants on the self-association and isomeric distribution of these complexes was also studied [32]. The surfactants used were the cationic detergent CPC (cetylpyridinium chloride; $Me(CH_2)_{15}(C_5H_5N)^+Cl^-$) and the nonionic surfactant of the chemical composition $C_{12}E_4$ (*i.e.*, C_iE_j, where C_i is $Me(CH_2)_{i-1}$ and E_j is $(OCH_2CH_2)_jOH$, $i=12$, $j=4$), containing a linear C_{13} alkyl chain with four ethyleneglycol groups attached at one end. The titrations of 10 mM solutions of the two Eu^{3+} complexes with the two surfactants were followed by ^{31}P-NMR (*Fig. 5* and *Fig. S8*[1])). The cationic detergent CPC drastically alters both the shifts and distribution of the stereoisomers of [Eu(DOTP*-OBu)]$^-$ (*Fig. 5*), while the nonionic $C_{12}E_4$ has no influence (data not shown). Upon increase of the CPC concentration, the various stereoisomers disappear gradually, and a single stereoisomer dominates, with a chemical shift δ of *ca.* 37. This new ^{31}P-NMR resonance is assigned to the [Eu(DOTP*-OBu)]$^-$ complex strongly bound at the surface of the cationic CPC micelles, through a strong coulombic interaction with the positively charged pyridinium ring and insertion of the butyl chains in the hydrophobic core of the micelles. Thus, it should be the (*S*,*S*,*S*,*S*) isomer, as it gives a single resonance and has the butyl side chains close together and pointing to the C_4 axis of the complex, as observed before with the [Ln(DOTP-Otfe)]$^-$ complex [32]. The observed shift results from a combination of the LIS and ring-current shifts due to the pyridinium rings. The absence of interaction with the nonionic surfactant, $C_{12}E_4$, up to a mol-equiv. ratio of 10:1, reflects the absence of the charge interaction due to the hydrophilic character of the tetraethyleneglycol chain.

The gradual addition of both the cationic CPC and the nonionic $C_{12}E_4$ surfactants has no significant effect on the ^{31}P-NMR spectrum of an aqueous [Eu(DOTP*-OEt)]$^-$ solution (*Fig. S8*[1])). The absence of interaction with the CPC micelles should result both from the stronger self-association of this complex, and from the absence of long alkyl chains in the complex, as its ethyl chains are too short to penetrate in the hydrophobic core of the micelles.

We also verified by ^{31}P-NMR that the presence of blood or serum albumin alters the isomer populations of [Eu(DOTP*-OEt)]$^-$ in favor of one isomer which preferentially

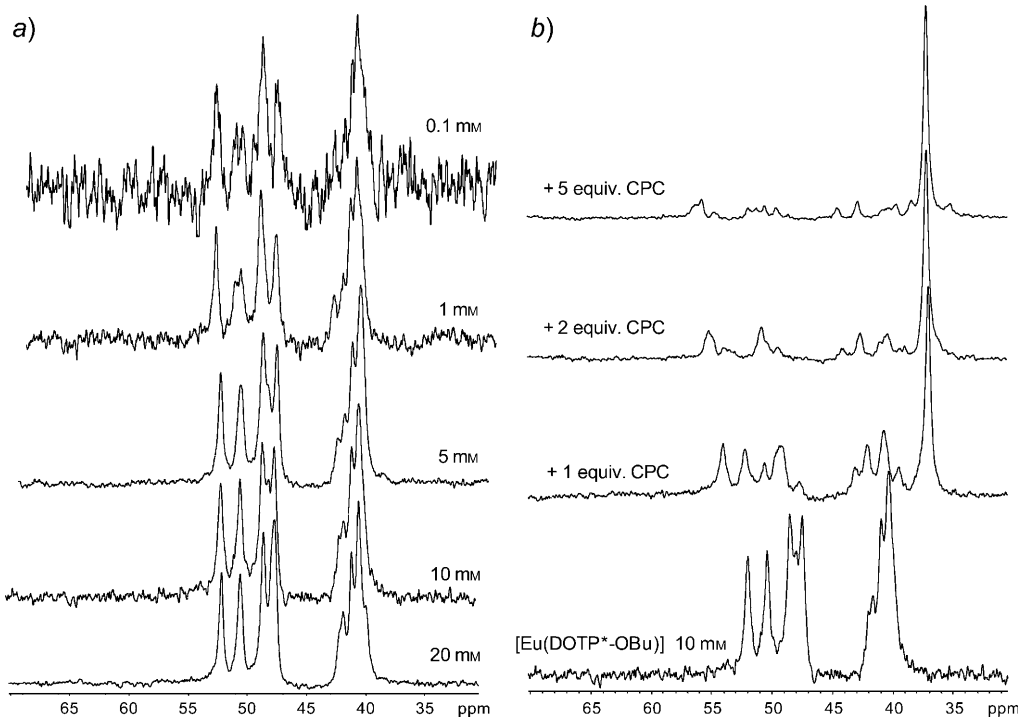

Fig. 5. *^{31}P-NMR Spectra of [Eu(DOTP*-OBu)]$^{-}$. a*) As a function of concentration (0.1 – 20.0 mM, pH 7.0, 298 K); *b*) upon addition of 1 – 5 mol equiv. of CPC.

interacts with albumin (data not shown). Also, dissolution of [Eu(DOTP*-OEt)]$^{-}$ in nonaqueous solvents, such as DMSO, DMF, or MeCN, causes large changes of the isomer populations and shifts (data not shown).

3.6.3. *EPR Studies.* The X-band EPR spectra of the [Gd(DOTP*-Et)]$^{-}$, [Gd(DOTP*-OEt)]$^{-}$, and [Gd(DOTP*-OBu)]$^{-}$ complexes in aqueous solution gave approximately *Lorentzian* lines with $g \approx 2.0$, and experimental peak-to-peak linewidths ΔH_{pp} which were dependent on the concentration of the complexes (*Table 3*). An increase of the linewidth is observed in all cases at concentrations higher than 1 mM, depending on the substituents, but it is quite large for 10 mM [Gd(DOTP*-OEt)]$^{-}$. In the case of the phosphinato complex [Gd(DOTP*-H)]$^{-}$, with the simplest substituent R = H, such an effect is not observed, indicating that the broadening of the EPR line in the substituted complexes results from their self-association in solution, possibly through interaction of the side chains at the P-atom of the pendant arms. Such a self-association process causes line broadening through spin-exchange interactions of the neighboring Gd^{3+} ions, which contribute to their transverse electronic relaxation rate ($1/T_{2e}$), determining the EPR line width (*Eqn. 6*, in which the symbols have their usual meaning) [43].

$$\frac{1}{T_{2e}} = \frac{g_L \mu_B \pi \sqrt{3}}{h} \Delta H_{pp} \qquad (6)$$

Table 3. *X-Band EPR Linewidths of Some Gd^{3+} Complexes with DOTP* Derivatives as Ligands at the Concentrations 1, 5, and 10 mM in H_2O at 298 K and pH 7* (errors given in parenthesis)

	Concentration [mM]	ΔH_{pp} [mT]
[Gd(DOTP*-Et)]$^-$	1	23.4 (0.2)
	5	41.5 (0.2)
	10	51.6 (0.2)
[Gd(DOTP*-OEt)]$^-$	1	40.5 (0.5)
	5	42.5 (0.5)
	10	80.0 (0.2)
[Gd(DOTP*-OBu)]$^-$	1	32.9 (1.0)
	5	36.2 (1.6)
	10	40.0 (0.2)
[Gd(DOTP*-H)]$^-$	1	26.0 (0.2)
	5	27.5 (0.5)
	10	25.7 (0.2)

3.6.4. *Osmolality Studies.* The osmolality of solutions containing the ligands H_8DOTP, H_4DOTP*-Et, or their Eu^{3+} complexes [Eu(DOTP)]$^{5-}$ or [Eu(DOTP*-Et)]$^-$, was measured in aqueous solution in the 2.5 – 50 mM concentration range. The osmolality (*Osm*) which is the number of moles of solute per kg of solvent contributing to the osmotic pressure of the solution, can be represented by *Eqn. 7*, where ϕ is the osmotic coefficient correcting for the solution nonideality or ionic dissociation, n is the number of particles originating from the solute ionic dissociation, C_2 is the solute concentration (g solute/kg solvent), and M_2 is the solute molecular mass. *Fig. 6* shows the data obtained plotted as the (osmolality/C_2) ratio as a function of C_2. For the highest concentrations studied (C_2 values corresponding to more than 10 mM), the osmolality/C_2 ratio is independent of C_2, indicating that the quantity $\phi\ n/M_2$ does not change. However, at 2.5 mM, the ratio decreased sharply indicating a decrease in the apparent molecular mass M_2 of the solute. This provided further evidence for self-association at the higher concentrations.

$$Osm = \phi\ n\ C_2/M_2 \tag{7}$$

3.6.5. *Luminescence Studies.* The luminescence intensity of the [Tb(DOTP*-OEt)]$^-$ complex at 1.5 mM in aqueous solution, as measured at 544 nm, corresponding to the $^5D_4 \rightarrow {}^7F_5$ transition of Tb^{3+}, decreased in the presence of increasing concentrations of [Eu(DOTP*-OEt)]$^-$ (*Fig. S9*[1])), reflecting a dynamic quenching process involving collisions of the Tb^{3+} and Eu^{3+} complexes in solution. The corresponding *Stern–Volmer* plot, according to *Eqn. 8*, where I_o and I are the intensities in the absence and presence of the quencher Q = [Eu(DOTP*-OEt)]$^-$ with concentration [Q], and K_{SV} is a constant characteristic of the process, is not linear (*Fig. 7*). The luminescence quenching fraction $(I_0 - I)/I$ increased almost linearly up to [Q] $\approx$ 1 mM, corresponding to a collisional process with a constant $K_{SV} = 0.44 \pm 0.03$ mM^{-1}. However, above this concentration of the quencher, the plot becomes nonlinear, with a sharp decrease of the

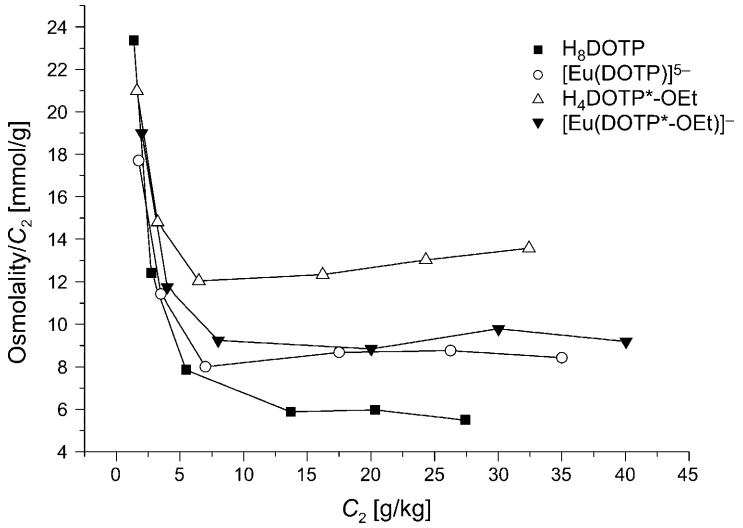

Fig. 6. *Plot of the osmolality/*C_2 *ratio as a function of the concentration* C_2 *for aqueous solutions of* H_8*DOTP* (■), H_4*DOTP*-OEt* (△), *and their* Eu^{3+} *complexes* [Eu(DOTP)]$^{5-}$ (○) *and* [Eu(DOTP*-OEt)]$^-$ (▼)

quenching efficiency, reflected in a decrease of K_{SV}, indicating aggregation of the [Ln(DOTP*-OEt)]$^-$ complexes at higher solution concentrations.

$$(I_0 - I)/I = K_{SV}\,[\mathrm{Q}] \tag{8}$$

4. Conclusions. – The present studies of the [Ln(DOTP*-Et)]$^-$, [Ln(DOTP*-OEt)]$^-$, and [Ln(DOTP*-OBu)]$^-$ complexes provided several new conclusions about their solution structures and aggregation. The ^{1}H- and ^{31}P-NMR spectra confirmed that all the [Ln(DOTP*-Et)]$^-$ complexes occur in solution overwhelmingly as the (*R*,*R*,*R*,*R*) diastereoisomer, with a very small contribution from the (*R*,*R*,*R*,*S*) (or (*S*,*S*,*S*,*R*)) form, while no such isomer preference is observed in the [Ln(DOTP*-OEt)]$^-$ and [Ln(DOTP*-OBu)]$^-$ complexes, which occur in solution as a complex mixture of isomers [31].

Plots for the separation of the pseudocontact and contact contributions to the ^{1}H and ^{31}P paramagnetic shifts for the [Ln(DOTP*-Et)]$^-$ series of complexes showed a break between Eu and Tb, reflecting a gradual structural change in the TSA coordination sphere, rather than a change of H_2O coordination, which should be zero for most of the Ln series. However, a fitting procedure of the experimental G_i values with a structural model gave very poor results. The negative sign of the experimental G_i values obtained for the H(7) and H(8) protons of the Et chains point to a (*R*,*R*,*R*,*R*) configuration of the major isomer. Fitting the LIS values of the [Yb(DOTP*-Et)]$^-$ complex to structural models also supported the presence of the (*R*,*R*,*R*,*R*) isomer.

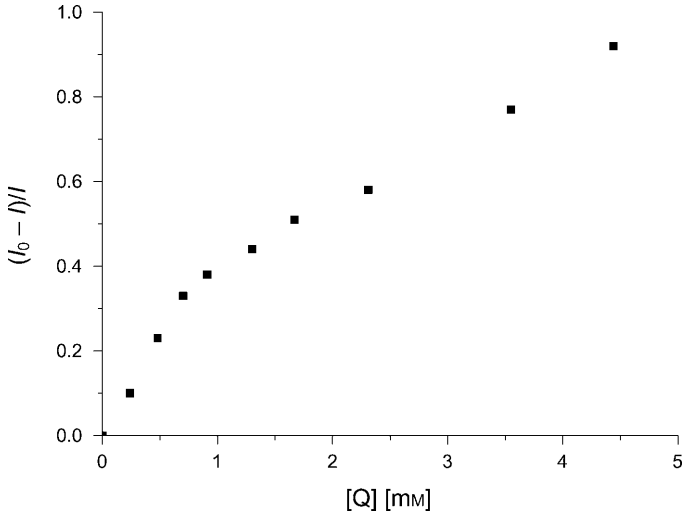

Fig. 7. Stern–Volmer *plot for 1.5 mM [Tb(DOTP*-OEt)]$^{-}$ in aqueous solution in the absence and presence of increasing concentrations of the quencher Q = [Eu(DOTP*-OEt)]$^{-}$*

The ^{31}P-NMR spectra allowed to conclude that the relative populations of the various isomers present in solution for the tetraazatetrakisphosphonato esters [Eu(DOTP*-OBu)]$^{-}$ and [Eu(DOTP*-OEt)]$^{-}$ change sharply with their concentration, indicating self-association at and above 5 mM. The EPR, osmometry, and luminescence-quenching data support such a self-association process of the complexes, which is largest for [Eu(DOTP*-OEt)]$^{-}$. This indicates that the hydrophobic intermolecular interactions of the side chains of the complexes in the aggregates strongly influence their isomer configuration about the P-atoms in solution. These interactions are disturbed by addition of the cationic detergent CPC to [Eu(DOTP*-OBu)]$^{-}$ solutions but not to [Eu(DOTP*-OEt)]$^{-}$, and also not for both complexes when the neutral surfactant $C_{12}E_4$ is added. When CPC is added to [Eu(DOTP*-OBu)]$^{-}$, all the isomers present disappear, except for the (*S*,*S*,*S*,*S*) isomer, which selectively binds to the cationic micelle surface through strong coulombic interaction with the positively charged pyridinium ring of CPC and insertion of the butyl chains in the hydrophobic core of the micelles.

This work was supported by the *Foundation of Science and Technology* (*F.C.T.*), Portugal (project PTDC/QUI/70063/2006 and grant SFRH/BPD/35005/2007 to *G.A.P.*), *FEDER*, and the *Robert A. Welch Foundation* (AT-584). The *Varian-VNMRS-600* NMR spectrometer is part of the National NMR Network and was acquired with funds from *Fundação para a Ciência e a Tecnologia* and *FEDER*. We thank *P. M. Coxito* for help running the SHIFT ANALYSIS program. The study was carried out within the framework of the *COST* Action D38 'Metal-Based Systems for Molecular Imaging Applications' and the *EU-FP6* 'Network of Excellence', European Molecular Imaging Laboratory (EMIL, No. LSHC-2004-503569).

Supplementary Information[1]). Figures showing the ^{1}H-NMR spectra of [La(DOTP*-Et)]$^{-}$ and [Lu(DOTP*-Et)]$^{-}$ complexes in D_2O (10 mM, pH 7.0, 298 K) (*Fig. S1*); the ^{31}P-2D-EXSY spectra of the [Nd(DOTP*-Et)]$^{-}$ complex (pH 7.0, 298 K, D_2O) at 0, 10, 25, and 50 ms mixing time (*Fig. S2*); plots of

the ^{1}H and ^{31}P LIS data for separation of contact and pseudocontact contributions for the (*R*,*R*,*R*,*R*) (or (*S*,*S*,*S*,*S*)) isomer of [Ln(DOTP*-Et)]$^-$ complexes according to *Eqn. 4* (*Fig. S3*) and *Eqn. 5* (*Fig. S4*); ^{31}P-NMR spectra of [Ln(DOTP*-OBu)]$^-$ complexes (10 mM, pH 7.0, 298 K) (*Fig. S5*); ^{1}H-NMR spectra of [La(DOTP*-OBu)]$^-$ and [Lu(DOTP*-OBu)]$^-$ complexes in D_2O (10 mM, pH 7.0, 298 K) (*Fig. S6*); ^{1}H-NMR spectra of some [Ln(DOTP*-OBu)]$^-$ complexes (10 mM, pH 7.0, 298 K, D_2O) (Ln = Ce and Sm) (*Fig. S7*); ^{31}P-NMR spectra of [Eu(DOTP*-OEt)]$^-$; A) as a function of concentration (0.1 – 25.0 mM, pH 7.0, 298 K); B) upon addition of CPC; C) upon addition of $C_{12}E_4$ (*Fig. S8*); luminescence band at 544 nm of the 1.5 mM [Tb(DOTP*-OEt)]$^-$ complex in aqueous solution in the absence and presence of increasing concentrations of [Eu(DOTP*-OEt)]$^-$ (*Fig. S9*); Table containing the ^{1}H and ^{31}P LIS values for the [Ln(DOTP*-Et)]$^-$ complexes (10 mM; pH 7.0; 298 K) (*Table S1*); Table containing the *F* and *G* parameters for the protons and ^{31}P nuclei obtained from the plots of separation of contact and pseudocontact contributions to the observed ^{1}H and ^{31}P LIS in the the (*R*,*R*,*R*,*R*) (or (*S*,*S*,*S*,*S*)) isomer of [Ln(DOTP*-Et)]$^-$ complexes according to *Eqn. 5* (*Table S2*).

REFERENCES

[1] S. Aime, M. Fasano, E. Terreno, *Chem. Soc. Rev.* **1998**, *27*, 19.
[2] 'The Chemistry of Contrast Agents in Medical Magnetic Resonance Imaging', Eds. A. E. Merbach and É. Tóth, Wiley, Chichester, 2001.
[3] 'Contrast Agents I. Magnetic Resonance Imaging', Ed. W. Krause, 'Topics in Current Chemistry', Vol. 221, Springer, 2002.
[4] P. Caravan, J. J. Ellison, T. J. McMurry, R. B. Lauffer, *Chem. Rev.* **1999**, *99*, 2293.
[5] S. Aime, M. Botta, E. Terreno, *Adv. Inorg. Chem.* **2005**, *57*, 173.
[6] P. Caravan, *Chem. Soc. Rev.* **2006**, *35*, 512.
[7] A. Nonat, C. Gateau, P. H. Fries, M. Mazzanti, *Chem. – Eur. J.* **2006**, *12*, 7133.
[8] M. Botta, *Eur. J. Inorg. Chem.* **2000**, 399.
[9] F. Avecilla, J. A. Peters, C. F. G. C. Geraldes, *Eur. J. Inorg. Chem.* **2003**, 4179.
[10] C. F. G. C. Geraldes, R. D. Brown III, W. P. Cacheris, S. H. Koenig, A. D. Sherry, M. Spiller, *Magn. Reson. Med.* **1989**, *9*, 94.
[11] S. Aime, M. Botta, D. Parker, J. A. G. Williams, *J. Chem. Soc., Dalton Trans.* **1996**, 17.
[12] S. Aime, M. Botta, E. Terreno, P. L. Anelli, F. Uggeri, *Magn. Reson. Med.* **1993**, *30*, 583.
[13] C. F. G. C. Geraldes, A. D. Sherry, W. P. Cacheris, *Inorg. Chem.* **1989**, *28*, 3336.
[14] R. Delgado, L. C. Siegfried, T. A. Kaden, *Helv. Chim. Acta* **1990**, *73*, 140.
[15] W. P. Cacheris, S. K. Nickle, A. D. Sherry, *Inorg. Chem.* **1987**, *26*, 958.
[16] C. F. C. G. Geraldes, A. D. Sherry, G. E. Kiefer, *J. Magn. Reson.* **1992**, *97*, 290.
[17] I. Lazar, D. C. Hrncir, W. D. Kim, G. E. Kiefer, A. D. Sherry, *Inorg. Chem.* **1992**, *31*, 4422.
[18] A. D. Sherry, J. Ren, J. Huskens, E. Brücher, É. Tóth, C. F. C. G. Geraldes, M. M. C. A. Castro, W. P. Cacheris, *Inorg. Chem.* **1996**, *35*, 4604.
[19] J. Ren, A. D. Sherry, *Inorg. Chim. Acta* **1996**, *246*, 331.
[20] A. D. Sherry, C. R. Malloy, F. M. H. Jeffrey, W. P. Cacheris, C. F. G. C. Geraldes, *J. Magn. Reson.* **1988**, *76*, 528.
[21] D. C. Buster, M. M. C. A. Castro, C. F. G. C. Geraldes, C. R. Malloy, A. D. Sherry, T. C. Siemers, *Magn. Reson. Med.* **1990**, *15*, 25.
[22] C. R. Malloy, D. C. Buster, M. M. C. A. Castro, C. F. G. C. Geraldes, F. M. H. Jeffrey, A. D. Sherry, *Magn. Reson. Med.* **1990**, *15*, 33.
[23] P. M. Winter, V. Seshan, J. D. Makos, A. D. Sherry, C. R. Malloy, N. Bansal, *J. Appl. Physiol.* **1998**, *85*, 1806.
[24] J. D. Makos, C. R. Malloy, A. D. Sherry, *J. Appl. Physiol.* **1998**, *85*, 1800.
[25] F. C. Alves, P. Donato, A. D. Sherry, A. Zaheer, S. Zhang, A. J. Lubag, M. E. Merritt, R. E. Lenkinski, J. V. Frangioni, M. Neves, M. I. M. Prata, A. C. Santos, J. J. P. de Lima, C. F. G. C. Geraldes, *Invest. Radiol.* **2003**, *38*, 750.
[26] X. Li, S. Zhang, P. Zhao, Z. Kovacs, A. D. Sherry, *Inorg. Chem.* **2001**, *40*, 6572; P. Caravan, M. T. Greenfield, X. Li, A. D. Sherry, *Inorg. Chem.* **2001**, *40*, 6580.

[27] C. F. G. C. Geraldes, A. D. Sherry, I. Lázár, A. Miseta, P. Bogner, E. Berenyi, B. Sumegi, G. E. Kiefer, K. McMillan, F. Maton, R. N. Muller, *Magn. Reson. Med.* **1993**, *30*, 696.
[28] M. Murru, D. Parker, G. Williams, A. Beeby, *J. Chem. Soc., Chem. Commun.* **1993**, 1116.
[29] J. Rohovec, P. Vojtíšek, P. Hermann, J. Mosinger, Z. Žák, I. Lukeš, *J. Chem. Soc., Dalton Trans.* **1999**, 3585.
[30] a) S. Aime, A. S. Batsanov, M. Bota, J. A. K. Howard, D. Parker, K. Senanayake, G. Williams, *Inorg. Chem.* **1994**, *33*, 4696; b) S. Aime, A. S. Batsanov, M. Botta, R. S. Dickins, S. Faulkner, C. E. Foster, A. Harrison, J. A. K. Howard, J. M. Moloney, T. J. Norman, D. Parker, L. Royle, J. A. G. Williams, *J. Chem. Soc., Dalton Trans.* **1997**, 3623; c) R. L. Luck, C. L. Maupin, D. Parker, J. P. Riehl, J. A. G. Williams, *Inorg. Chim. Acta* **2001**, *317*, 331.
[31] Z. Kotková, G. A. Pereira, K. Djanashvili, J. Kotek, J. Rudovský, P. Hermann, L. Vander Elst, R. N. Muller, C. F. G. C. Geraldes, I. Lukeš, J. A. Peters, *Eur. J. Inorg. Chem*. **2009**, 119.
[32] W. D. Kim, G. E. Kiefer, J. Huskens, A. D. Sherry, *Inorg. Chem.* **1997**, *36*, 4128.
[33] L. Burai, R. Király, I. Lázár, E. Brücher, *Eur. J. Inorg. Chem.* **2001**, 813.
[34] I. Lazar, A.-D. Sherry, R. Ramasamy, E. Brücher, R. Kiraly, *Inorg. Chem.* **1991**, *30*, 5016.
[35] A. Barge, G. Cravotto, E. Gianolio, F. Fedeli, *Contrast Media Mol. Imaging* **2006**, *1*, 184.
[36] J. H. Forsberg, R. M. Delaney, Q. Zhao, G. Harakas, R. Chandran, *Inorg. Chem.* **1995**, *34*, 3705.
[37] M. R. Willcott III, R. E. Lenkinski, R. E. Davis, *J. Am. Chem. Soc.* **1972**, *94*, 1742.
[38] S. Aime, M. Botta, M. Fasano, M. P. M. Marques, C. F. G. C. Geraldes, D. Pubanz, A. E. Merbach, *Inorg. Chem.* **1997**, *36*, 2059.
[39] J. A. Peters, J. Huskens, D. J. Raber, *Prog. Nucl. Magn. Reson. Spectrosc.* **1996**, *28*, 283.
[40] C. N. Reilley, B. W. Good, R. D. Allendoerfer, *Anal. Chem.* **1976**, *48*, 1446.
[41] P. Vojtíšek, P. Cígler, J. Kotek, J. Rudovský, P. Hermann, I. Lukeš, *Inorg. Chem.* **2005**, *44*, 5591.
[42] J. Rohovec, M. Kývala, P. Vojtíšek, P. Hermann, I. Lukeš, *Eur. J. Inorg. Chem.* **2000**, 195.
[43] J. Kotek, P. Lebdusková, P. Hermann, L. Vander Elst, R. N. Muller, C. F. G. C. Geraldes, T. Maschmeyer, I. Lukeš, J. A. Peters, *Chem. – Eur. J.* **2003**, *9*, 5899.

Received May 4, 2009